Chapter 4
A Highly Hydrogen Permeable Silica Membrane Supported on Porous Alumina

4.1. Introduction

In previous chapters, the synthesis of a highly hydrogen selective membrane formed by the deposition of a silica layer on top of a Vycor glass substrate was discussed. In this chapter, the preparation of a composite membrane using a porous alumina support is described. This membrane showed a high hydrogen permeance of the order of 10^{-7} mol m^{-2} s^{-1} Pa^{-1} at 873 K with selectivity of hydrogen over CH_4, CO, and CO_2 above 2000. The notable result is that the permeance of hydrogen is one order of magnitude higher than that of the silica membrane obtained on the porous Vycor support. The membranes were examined using Field Emission Scanning Electron Microscopy (FESEM) to give their cross-sectional morphology and Atomic Force Microscopy (AFM) to show their surface structure. The gas permeation properties of the membranes were discussed, and the transport of He and H_2 gases through the silica membrane was analyzed using the statistical gas permeation mechanism described in Chapter 3.

4.2. Experimental

The silica/alumina membrane was prepared by depositing a thin silica layer on a porous γ-alumina support by the thermal decomposition of tetraethylorthosilicate (TEOS) at 873 K in an argon stream. The membrane support used in this study was purchased from US Filter (Part No. S700-0011), and had a tubular geometry with an outside diameter of 10 mm and a thickness of 1.5 mm. This membrane support had a multi-layered structure consisting of a coarse α-Al_2O_3 tube coated with finer layers of α-Al_2O_3 and an inner top layer of γ-Al_2O_3 of average 5 nm pore size. A 5 cm section of the alumina membrane support was connected at both ends to two pieces of dense alumina tubing using a high temperature glass glaze (Duncan, IN, Part No. 1001). Gas tight connections between the membrane support and the dense tubing were obtained after 0.5 h of thermal treatment at 1150 K.

After the joint connection, an additional γ-Al_2O_3 layer was introduced on top of the existing γ-Al_2O_3 layer of the alumina support to reduce defects or pinholes that give rise to a low hydrogen selectivity in the silica layer. A 0.05 M dispersion of boehmite (γ-AlOOH) sol was prepared following the method reported by Uhlhorn [1]. Aluminum tri-sec-butoxide (Aldrich, 97%) was added to boiling water with vigorous stirring, and 0.07 mole HNO_3 per mole butoxide was added. This colloidal solution was boiled until most of the butanol was evaporated, then was refluxed for 20 h. A polyvinylalcohol (PVA, Fluka, M.W. 72000) solution was prepared separately by adding 3.5 g of PVA to 100 cm^3 of boiling water followed by 5 cm^3 of 1 M HNO_3. The PVA solution was then refluxed for 4 h. A final 0.05 M boehmite sol was prepared after adding 660 cm^3 of the PVA solution per mol of boehmite followed by stirring for 3 h at 353 K. The inside of the alumina support tube was dip coated with the 0.05 M boehmite sol for 10 s, dried for 24 h at room temperature, and then calcined at 873 K for 24 h (heating rate 1 K min^{-1}).

Unsupported γ-Al_2O_3 films were also prepared by drying the boehmite sol in polypropylene Petri dishes at room temperature. The obtained gel films were calcined at the same temperature as used for the membrane synthesis (873 K) for various times (3, 24, 72 h) to determine the resulting pore size distributions of the γ-Al_2O_3.

For the CVD of the silica layer, the alumina support ensemble was installed concentrically inside a piece of glass tubing of 14 mm inside diameter using machined Swagelok fittings with Teflon ferrules. After placing the assembly in an electric furnace, argon gas flows were introduced on the outer shell side (19 μmol s^{-1}) and inner tube side (15 μmol s^{-1}) of the reactor (flow rates in μmol s^{-1} may be converted to cm^3 min^{-1} (NTP) by multiplying by 1.5), and the temperature was raised to 873 K. A flow of tetraethylorthosilicate (TEOS, Aldrich, 98%) was introduced on the inside of the porous alumina substrate through a bubbler (at 298 K) using argon (4 μmol s^{-1}) as a carrier gas. This stream was mixed with the tube stream of argon before introducing it to the tube side to produce a stream with a TEOS concentration of 0.02 mol m^{-3} (0.045 mol %). The synthesis of the silica membrane was studied by varying the silica deposition time. The CVD process was interrupted at various times and the permeances of H_2, CH_4, CO, and CO_2 were measured at those different deposition times at 873 K

After preparation of the membrane, general gas permeation measurements were conducted in the temperature range of 373 – 873 K by flowing 40 μmol s^{-1} of a pure gas at 70 kPa through the inner tube. The permeation rate of each gas exiting from the shell side of the reactor assembly was measured with a sensitive bubble flow meter at atmospheric pressure. The permeance of gas was obtained from the expression $Q_i = F_i / A \Delta P_i$, where Q_i is the permeance (mol m^{-2} s^{-1} Pa^{-1}) of species i, F_i is the gas flow rate on the shell side (mol s^{-1}), A is the surface area (m^2) of the membrane section, and ΔP_i is the pressure difference (Pa) between the shell and tube side. For higher sensitivity the permeance of the gases was also measured with a gas chromatograph (GC) equipped with a thermal conductivity detector (SRI, Model 8610B). The tube side gas flow rates and pressure conditions were the same as above, however, on the shell side an argon flow was introduced as a sweep gas for the permeated gas. The shell side outlet gas flow rate was measured using a bubble flow meter, and the flow was injected into the GC to obtain the concentration of the permeated gas. The permeance was then calculated using the outlet gas flow rate and the concentration of the permeated gas on the shell side.

Cross-sectional structures of the alumina support substrate and the silica membrane were characterized using a Field Emission Scanning Electron Microscope (FESEM, Leo 1550). The samples were prepared by mechanically breaking the membranes after putting them into liquid nitrogen for 60 s. The samples were then introduced into the electron microscope and coated with gold by sputtering. The multilayered structure of the alumina support membrane substrate was examined, and the thickness of the deposited silica layer of the silica membrane was obtained from high resolution cross-sectional photos. The inner surface structures of the fresh alumina support and silica membrane were also characterized using a multimode Atomic Force Microscope (AFM, Digital Instrument, Nanoscope III). A cantilever with a pyramidal tip of Si (Nanoprobe) was used as the probe sensor. The surface structures of the samples were examined in the tapping mode to obtain the topography.

4.3. Results and Discussion

The pore size distribution curves for the unsupported γ-Al_2O_3 films obtained from nitrogen desorption isotherms using the Barrett, Joyner and Halenda (BJH) method are shown in Figure 4.1. The results indicate that small pores were developed on the γ-Al_2O_3 films with a pore size range between 3 and 5 nm after 3 h of calcination at 873 K. The size of the pores increased with further calcination (24 h) to give a narrow unimodal pore size distribution with average pore size of 4.5 nm. The pore size and its distribution changed little after extended calcination (72 h) indicating that the pore structure of the γ-Al_2O_3 film became stable after 24 h.

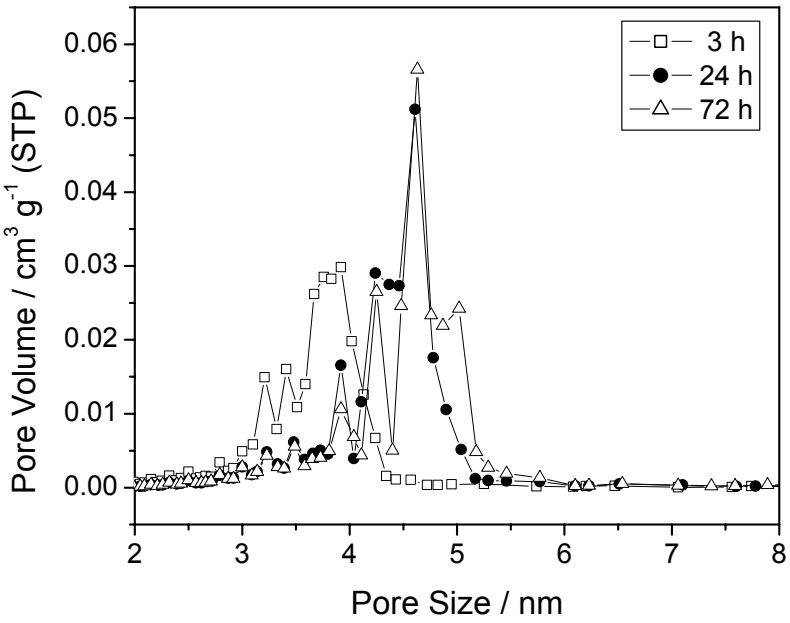

Figure 4.1. Pore size distribution of the unsupported γ-Al_2O_3 films.

4.3.1. Gas Transport through the Alumina Support

The alumina membrane used in this study as a support for the silica membrane preparation had a graded multilayer structure with large macropores in the α-Al_2O_3 support layers to small mesopores on the top γ-Al_2O_3 layer. The pore size of the support gradually

decreased layerwise from a few μm to an average pore size of 4.5 nm for the top γ-Al_2O_3 layer. The overall gas transport properties through this multilayered membrane were governed mainly by the transport properties of the top γ-Al_2O_3 layer. This was due to the larger gas diffusion resistance imposed by the small pores of the top layer compared to those of the large pores of the supporting layers. As discussed in Chapter 3 in gas transport through porous materials, Knudsen diffusion is a well known transport mechanism which occurs when the mean free path of gas molecules is much larger than the size of the pores [2]. In this regime, gas molecules diffuse through the pores by colliding with the pore walls under the driving force of a concentration gradient. The Knudsen permeance is given by:

$$Q = \frac{\varepsilon \, d_p}{\tau L}\left(\frac{8}{9\pi MRT}\right)^{\frac{1}{2}} \tag{4.1}$$

where Q is the permeance (mol m^{-2} s^{-1} Pa^{-1}), ε is the porosity, d_p is the pore diameter (m), τ is the tortuosity, L is the membrane thickness (m), R is the gas constant (8.314 J mol^{-1} K^{-1}), T is the temperature (K), and M is the molecular weight (kg mol^{-1}). The Knudsen diffusion equation predicts that gas permeance will have an inverse square root dependency on both the molecular weight and temperature. The ratio of the mean free paths of the gases used in this work (He, H_2, CH_4, CO, and CO_2) and the pore size of the γ-Al_2O_3 layer falls between 30 and 120, therefore the gas transport is expected to show Knudsen permeation characteristics.

The experimental gas permeance through the alumina membrane support was plotted versus the inverse square root of molecular weight at various temperatures, and the linear regression fits are presented in Figure 4.2. The results show a good linear dependence (r^2 = 0.997 to 0.999) confirming that the gas transport occurred mainly by Knudsen diffusion. The hydrogen selectivities over other gases (He: 1.36, CH_4: 2.40, CO: 3.25, and CO_2: 4.22) showed good agreement with the theoretical Knudsen selectivity values (He: 1.41, CH_4: 2.82, CO: 3.72, and CO_2: 4.67). The slightly lower experimental values for CH_4, CO and CO_2 are likely due to a small contribution of surface diffusion for theses condensable gases as occurred on the Vycor support [3]. The permeance data was also plotted versus the inverse square root of the temperature and the linear regression fits are presented in Figure 4.3. The results again show good fits (r^2 = 0.930 to 0.995) following the behavior expected from Knudsen transport.

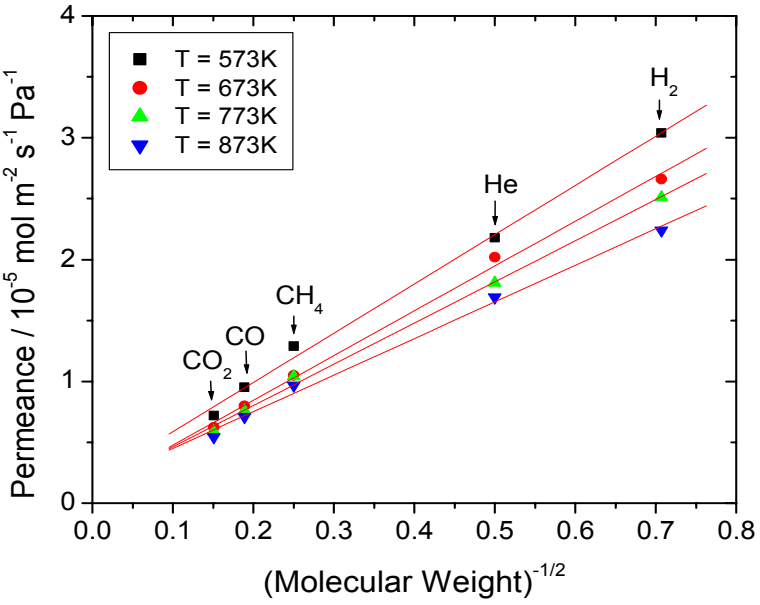

Figure 4.2. Gas permeance vs. molecular weight$^{-1/2}$ for the fresh alumina support.

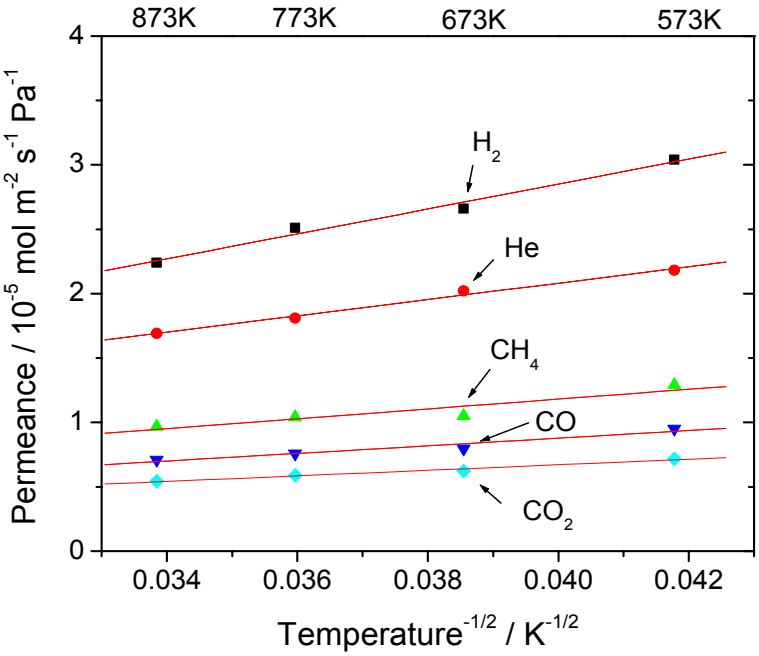

Figure 4.3. Gas permeance vs. temperature$^{-1/2}$ for the fresh alumina support.

4.3.2. Gas Transport through the Silica Membrane

The evolution of the gas permeance on the silica membrane was measured at 873 K as a function of the silica deposition time to monitor the formation of the silica layer on the membrane support. The results are shown in Figure 4.4. Initially, the fresh alumina support showed very high permeance for all the gases ($H_2 = 2.2 \times 10^{-5}$, $CH_4 = 9.7 \times 10^{-6}$, $CO = 7.1 \times 10^{-6}$, $CO_2 = 5.4 \times 10^{-6}$ mol m^{-2} s^{-1} Pa^{-1}). The permeance of all the gases decreased with silica deposition time. For hydrogen, the permeance decreased rapidly after 3 h of silica deposition to the order of 10^{-7} mol m^{-2} s^{-1} Pa^{-1}, and then decreased slowly with further silica deposition. In contrast, the permeances of CH_4, CO, and CO_2 showed a continuous and rapid drop with silica deposition. After 12 h of deposition the permeance of hydrogen remained at 1.2×10^{-7} mol m^{-2} s^{-1} Pa^{-1}, whereas the permeance of other gases dropped off significantly ($CH_4 = 4.3 \times 10^{-11}$, $CO = 6.7 \times 10^{-11}$, $CO_2 = 8.0 \times 10^{-11}$ mol m^{-2} s^{-1} Pa^{-1}).

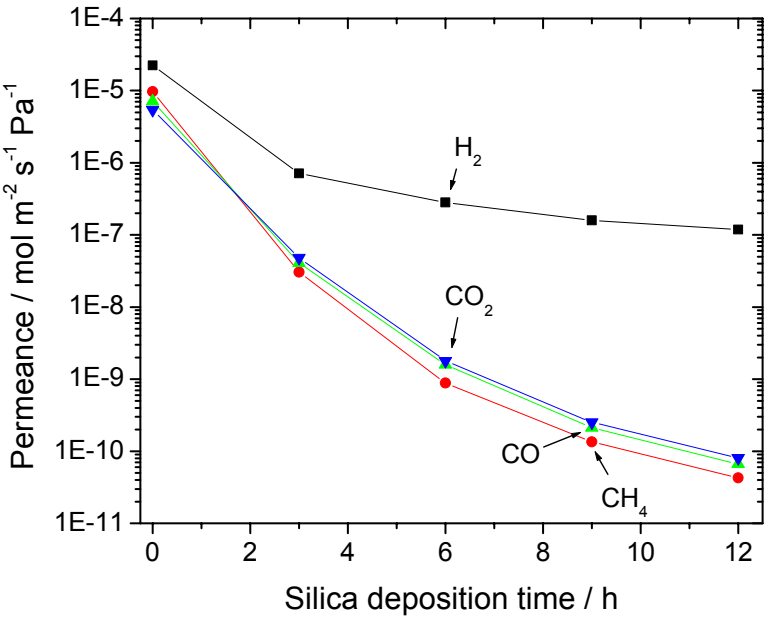

Figure 4.4. Gas permeance vs. silica deposition tiem

The results indicate that a complete silica layer was formed on the alumina support after 12 h of deposition, and that the layer was selective for H_2 transport while significantly excluding passage of CH_4, CO, and CO_2 through the membrane. Before the silica deposition, the permeance order

of the gases through the alumina support was $H_2 > CH_4 > CO > CO_2$ showing an inverse dependence on the molecular weight of the gases, in agreement with the Knudsen diffusion mechanism. However, after 3 h of silica deposition the permeance order changed to $H_2 > CO_2 > CO > CH_4$, which followed molecular size (H_2 = 0.289 nm, CO_2 = 0.33 nm, CO = 0.376 nm, CH_4 = 0.38 nm [4]), and this order was retained with further silica deposition. This gives evidence that the mechanism of molecular differentiation by the silica layer is through size selectivity.

The hydrogen selectivity over other gases is shown as a function of hydrogen permeance in Figure 4.5. On the fresh alumina support the selectivity for hydrogen was low for all the gases. As discussed in the previous section, the selectivity was characteristic of Knudsen diffusion. After 3 h of silica deposition the selectivity for hydrogen showed a slight increase accompanied by a large decrease in H_2 permeance from the order of 10^{-5} to 10^{-7} mol m^{-2} s^{-1} Pa^{-1}. The H_2 selectivity then increased rapidly with further silica deposition, with only a relatively small drop in hydrogen permeance. In this regime the increase of H_2 selectivity followed a log linear relation with the silica deposition. After 12 h of silica deposition the hydrogen selectivity of the membrane increased to over 1000 for all the gases (CH_4: 2800, CO: 1800, CO_2: 1500).

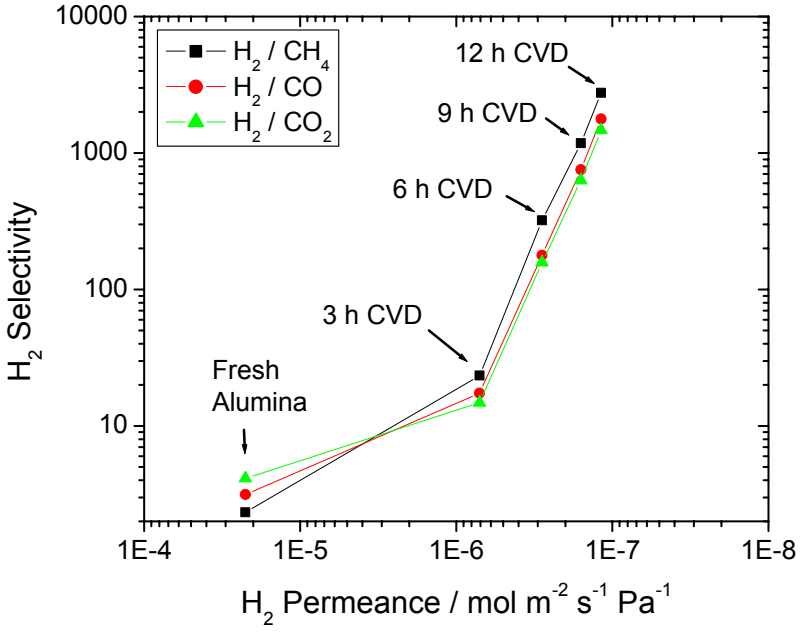

Figure 4.5. Selectivity of hydrogen vs. H_2 permeance.

The temperature dependence of small gas transport through the silica membrane obtained after 12 h of silica deposition was investigated by measuring the permeance of H_2 and He at various temperatures (373 – 873 K). It was found that the permeance of these gases through the silica membrane was activated, and increased with temperature. This differed from the permeance in the fresh alumina membrane support where the permeance decreased with temperature accordance with the Knudsen transport mechanism. The permeance order of these gases (He > H_2) followed molecular size (He = 0.26 nm, H_2 = 0.289 nm [4]) rather than the mass of the molecules (He = 4.0 au, H_2 = 2.01 au). The activation energies of permeation were obtained by fitting the experimental gas permeance data to an Arrhenius expression:

$$Q = Q_0 \exp(\frac{-E_a}{RT}) \qquad (4.2)$$

where Q is the permeance, Q_0 is the preexponential factor (mol m^{-2} s^{-1} Pa^{-1}), E_a is the activation energy (J mol^{-1}), R is the gas constant (8.314 J mol^{-1} K^{-1}), and T is the temperature (K). The fitting results and associated parameter values are shown in Figure 4.6 and Table 4.1. The experimental permeance data show good fits to the Arrhenius expression with an activation energy for H_2 of 14.8 kJ mol^{-1} and for He of 9.8 kJ mol^{-1}.

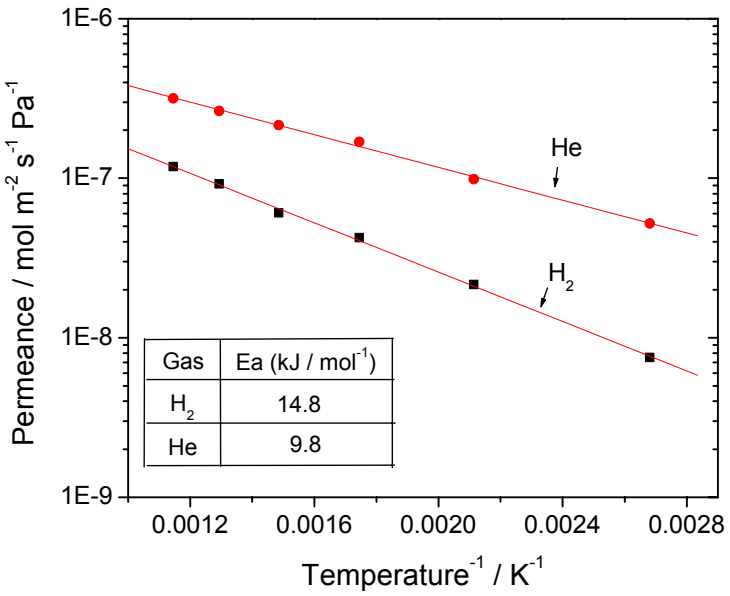

Figure 4.6. Arrhenius plot for the permeance of H_2 and He on the silica membrane.

Table 4.1. Best fit preexponential factor and activation energy for the Arrhenius gas permeation equation.

Gas	Preexponential factor Q_0 (mol m^{-2} s^{-1} Pa^{-1})	Activation energy E_a (kJ mol^{-1})	Sum of least squares $\Sigma(Q_{calc.} - Q_{expl.})^2$
H_2	9.0×10^{-7}	14.8	1.9×10^{-17}
He	1.2×10^{-6}	9.8	1.8×10^{-16}

4.3.3. Characterization of the Membranes

The cross-sectional images of the fresh alumina support and the silica membrane obtained by high resolution field emission scanning electron microscopy (FESEM) are shown in Figures 4.7a)-d). The cross-sectional photo of the fresh alumina support in Figure 4.7a) shows the multilayered graded structure of the support with different particle sizes for each Al_2O_3 layer, where the particle and pore size decrease gradually from the bottom of the figure (outside of the tube) to the top (inside of the tube). The top γ-Al_2O_3 layer with an average pore size of 4.5 nm had a thickness of about 4 to 5 μm. Figure 4.7b) is a magnified photo of the top γ-Al_2O_3 layer of the fresh alumina support.

The cross-sectional structure of the silica membrane is shown in Figures 4.7c)-d). The figures show a silica layer with a thickness of about 20 to 30 nm formed on top of the γ-Al_2O_3 layer after 12 h of silica deposition. The deposited silica layer shows good uniformity with a clear boundary with the support γ-Al_2O_3 layer. However, the cross-sectional morphology of the support γ-Al_2O_3 layer for the silica membrane is different from that of the fresh alumina support toward the bottom. This may have been caused by penetration of a small amount of silica into the porous γ-Al_2O_3 resulting in a different fracture property.

The surface structures of the fresh alumina support obtained from AFM measurements are shown in Figure 4.8a)-c). Figures 4.8a) and 4.8b) are phase images of the γ-Al_2O_3 surface

with scan sizes of 500 × 500 nm^2 and 250 × 250 nm^2, respectively, and Figure 4.8c) is the surface height image for Figure 4.8a). The phase images for the fresh alumina support show that the surface structure of the γ-Al_2O_3 layer has a rough and jagged topography with randomly distributed γ-Al_2O_3 particles. The size of the particles is not uniform, and has an approximate size range of 20 to 40 nm. Close examination of Figure 4.8b) indicates that the pore entrances are formed from the contact between three or four particles.

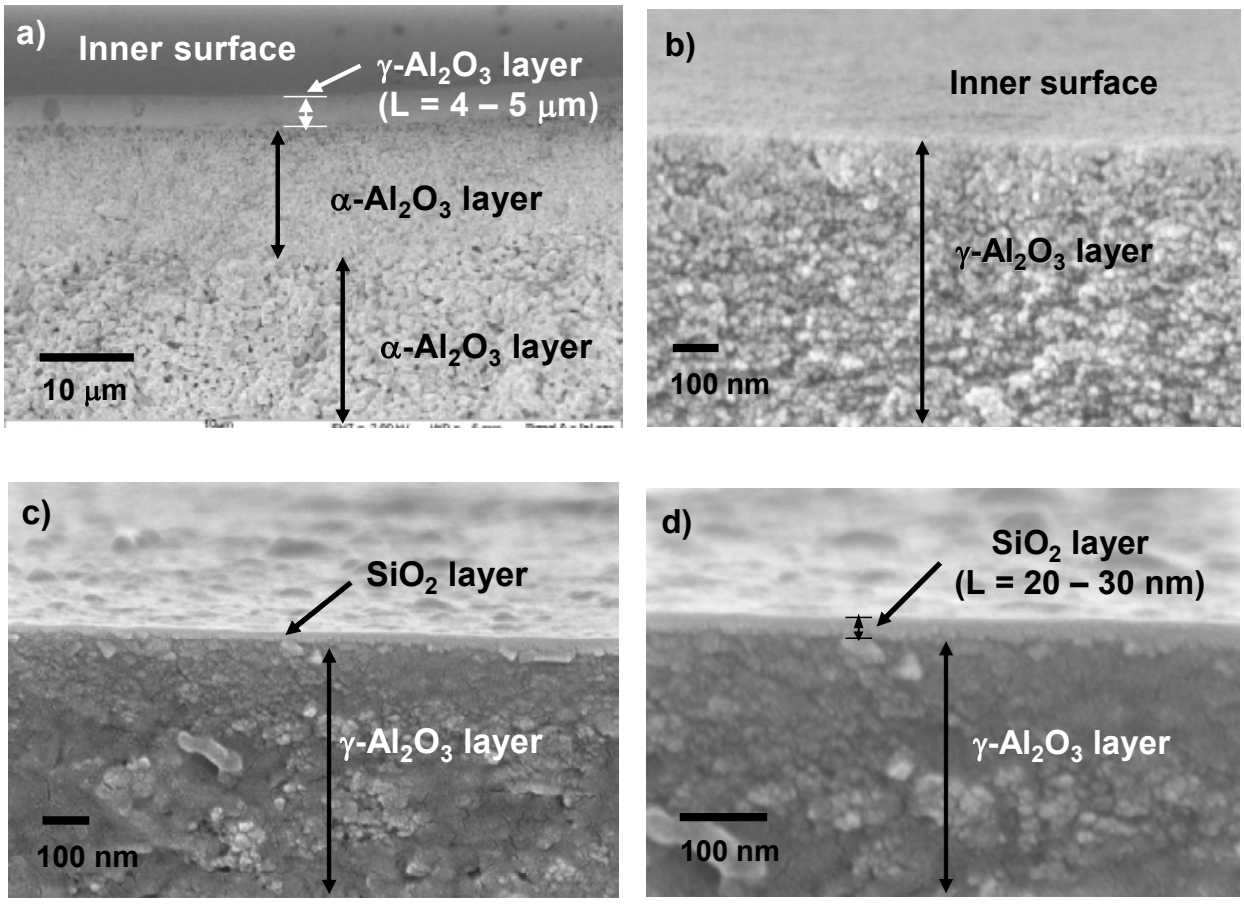

Figure 4.7. SEM cross-sectional photos of the fresh alumina support and the silica membrane.

a) Fresh alumina support (Mag. = 2K×) b) Fresh alumina support (Mag. = 100K×)

c) Silica membrane (Mag. = 100K×) d) Silica membrane (Mag. = 200K×)

The surface height image, 4.8c), shows a three dimensional view of the surface. The image confirms that the topography of the surface is rough and uneven in the scale of nanometers. The surface shows many sharp peaks and deep valleys, as would be expected for particles deposited on a surface.

The surface structure of the silica membrane after 12 h of silica deposition is shown in Figure 4.8d)-f). Figures 4.8d) and 4.8e) are phase images with scan size of 500 × 500 nm^2 and 250 × 250 nm^2, respectively, and Figure 4.8f) is a surface height image for the surface displayed in Figure 4.8d). The phase images show that the surface structure is smoother compared to that of the fresh γ-Al_2O_3 surface showing rounded particles due to the presence of the thin silica layer. The surface height image, 4.8f), clearly indicates a change of surface topography for the silica membrane, and also shows that the particles have become larger and smoother. The roughness of the surface structure decreased after silica deposition showing shallower peaks and valleys.

To compare the roughness of the surfaces the standard deviation of the height for the fresh alumina support and silica membrane surface was calculated by randomly taking eight cross-sections of the surface height images (Figures 4.8c) and 4.8f)). The standard deviation (σ) of the height is defined as:

$$\sigma = \sqrt{\frac{\Sigma(Z_i - Z_{ave})^2}{N}} \tag{4.3}$$

where Z_i is the height of peaks or valleys for the i^{th} data point, Z_{ave} is the average height, and N is the total number of data points. The calculated values were σ = 5.4 nm for the fresh alumina support surface and σ = 3.7 nm for the silica membrane surface. The results give a quantitative measure of the change of the surface roughness due to the deposition of the silica layer on the fresh γ-Al_2O_3 layer. The decrease of the surface roughness of the alumina surface with the silica layer gives insight about the nature of the deposition process. Schematic representations of the topography of the deposited layer are given in Figure 4.9a)-c). Figure 4.9a) shows the peaks and valleys of the alumina surface before silica deposition. Figure 4.9b) shows the surface with the silica layer in the case where deposition was uniform due to the flux of the CVD species in the direction normal to the surface.

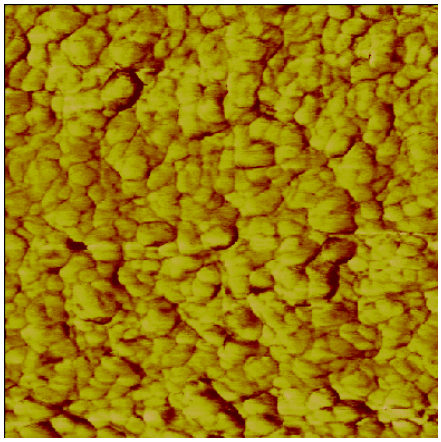

a) Fresh alumina (500 × 500 nm^2)

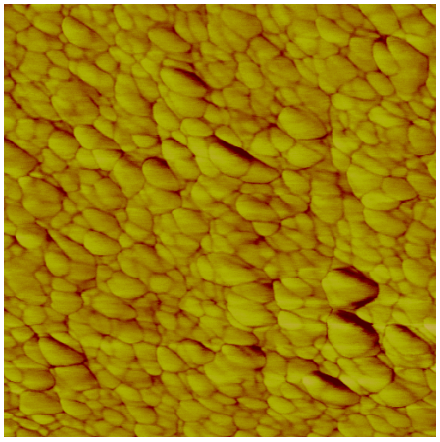

d) Silica membrane (250 × 250 nm^2)

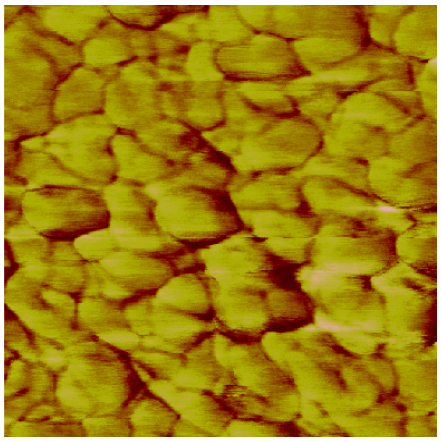

b) Fresh alumina (250 × 250 nm^2)

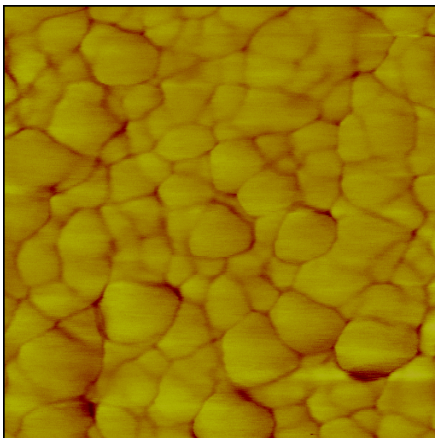

e) Silica membrane (250 × 250 nm^2)

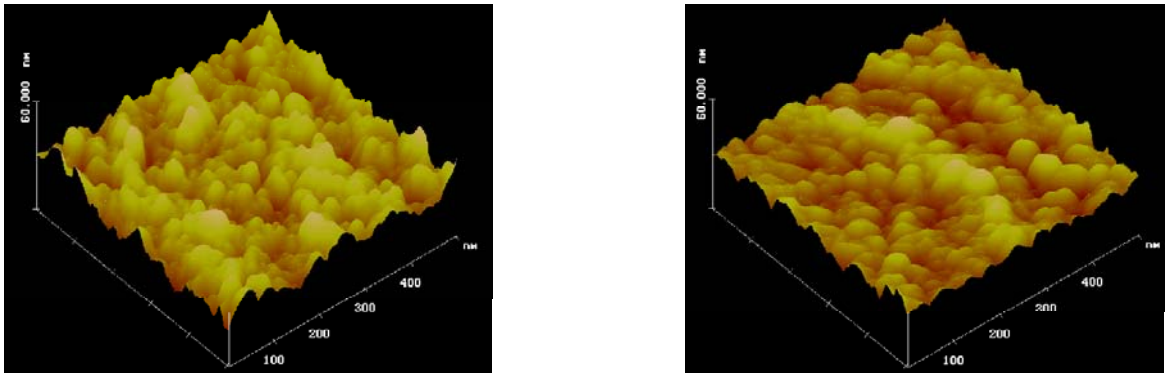

c) Fresh alumina (500 × 500 nm^2) **f) Silica membrane (500 × 500 nm^2)**

Figure 4.8. AFM images of the surface of the fresh γ-Al_2O_3 and the silica membrane.

a)-b) Phase image of the surface of the fresh alumina support

c) Height image of the surface of the fresh alumina surface

d)-e) Phase image of the surface of the silica membrane

f) Height image of the surface of the silica membrane

For this situation the thickness of the overlayer would be constant and no change in the height topography would be expected, so the σ value should remain constant. Figure 4.9c) show the case where preferential layer growth occurs in the valleys. The result is a smoothing of the roughness of the surface and a decrease in the σ value. In fact this is what is observed experimentally, and the result is reasonable. The average coordination at the sites in the valleys is higher than in the peaks, resulting in a larger number of bonding interaction as the silicate precursors are deposited. Conversely at the peaks the average coordination number is lower than in the valleys resulting in destabilization of the silica film precursors. These effects give rise to preferential filling of the valley sites. This mechanism also suggests that there is some mobility of the silica species on the surface of the membrane.

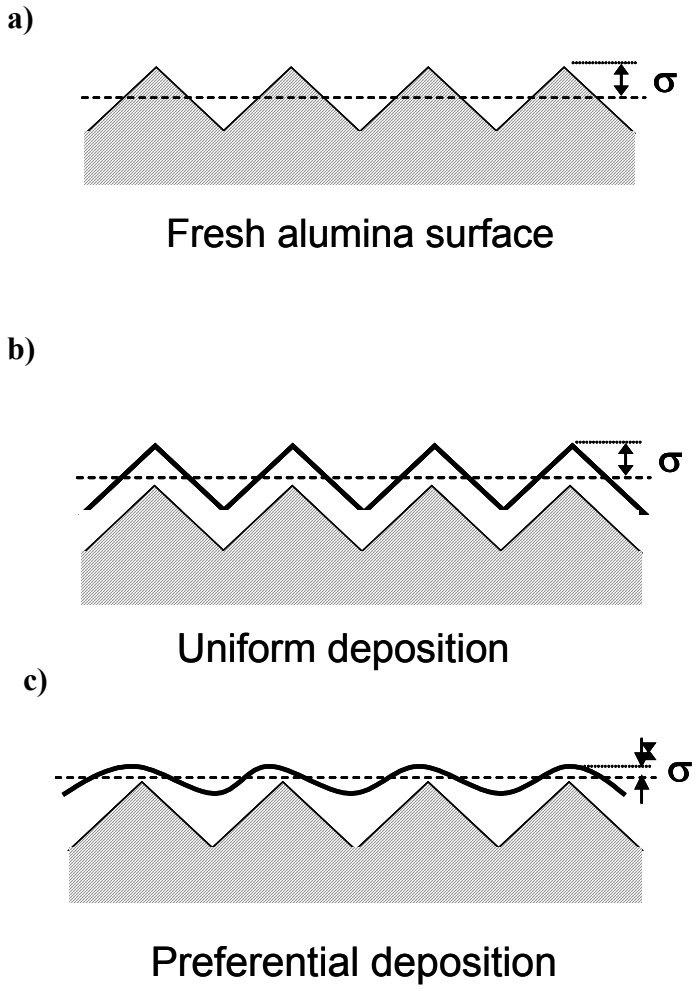

Figure 4.9. Schematic representations of uniform and preferential film deposition.

4.3.4. Mechanism of H_2 and He Permeation through the Silica Membrane

In Chapter 3, it was shown that the gas permeation characteristics through the silica membrane layer obtained by CVD on a porous Vycor support were similar to those for vitreous silica glasses. It was found in that work that a uniform and defect-free silica layer was formed by CVD which allowed permeation of only gas molecules of small size (He = 0.26 nm, Ne = 0.275 nm, H_2 = 0.289 nm [4]) while excluding the transport of gas molecules of large dimensions (CO_2 = 0.33 nm, CO = 0.376 nm, CH_4 = 0.38 nm). This could be explained from the structure of vitreous silica glasses which had been described as a disordered form of b-cristobalite that contains 5, 6, 7 and 8 membered rings, in which solubility sites are approximately 0.3 nm in

diameter [5]. The restricted size of the solubility sites in the silica matrix structure allows sorption of the small gas molecules while restricting sorption of the large gas molecules by size differentiation. The mechanism of small gas transport through the silica membrane is molecular diffusion, in which gas molecules enter into the solubility sites and then diffuse through the silica structure by jumping to adjacent solubility sites under the driving force of a concentration gradient. A few studies have been reported in the literature describing the sorption and diffusion of small molecules in silica glass using a statistical approach [6-8]. A statistical monatomic gas permeance model for silica glass has been presented [6]:

$$Q = \frac{1}{6L}\left(\frac{d^2}{h}\right)\left(\frac{h^2}{2\pi m k T}\right)^{\frac{3}{2}} \frac{(N_S / N_A)}{(e^{h\nu^*/2kT} - e^{-h\nu^*/2kT})^2} e^{-\Delta E_K/RT} \qquad (4.4)$$

where Q is the permeance (mol m^{-2} s^{-1} Pa^{-1}), L is the thickness of the diffusion layer (m), d is the jump distance (m), h is Plank's constant, k is Boltzmann's constant, m is the mass of the molecules, N_s is the number of solubility sites available per m^3 of glass volume, N_A is Avogadro's number, ν^* is the vibrational frequency of the gas molecules at the doorway sites, R is the gas constant, T is the temperature, and ΔE_K is the activation energy for permeation. This permeance model can be applied for hydrogen in the same form assuming no loss of rotational freedom at the doorway sites.

The experimental permeance of He and H_2 through the silica membrane obtained in this study was analyzed using the statistical gas permeance mechanism (Equation 4.4). The model equation has three adjustable parameters: the number of solubility sites, N_s, the vibrational frequency of molecules at the doorway sites, ν^*, and the activation energy for permeation (ΔE_K). A three parameter optimization was carried out for N_s, ν^*, and ΔE_K to find the best-fit parameter values for the experimental gas permeance data. An optimization program was written in Fortran using Newton's method [9]. The thickness of the silica layer, L, used was 20 nm which was obtained from the SEM experiments. The jump distance, d, was taken to be 0.3 nm which is the size of the solubility sites of β-cristobalite [10]. The results of the numerical fitting are presented in Figure 4.10. The calculations show excellent agreement between the model analysis and experimental permeance data with a permeance order of He > H_2 which is the same as that for silica glass [11-14]. This is an unusual order from the standpoint of Knudsen diffusion as the

molecular weight of He (4.0 au) is twice as large as that of H_2 (2.01 au), but is well explained by the statistical jump mechanism. Basically, the smaller size of He allows its accommodation in a larger number of solubility sites than H_2 and also results in a smaller jump barrier. The results of the calculations are detailed in the following paragraph.

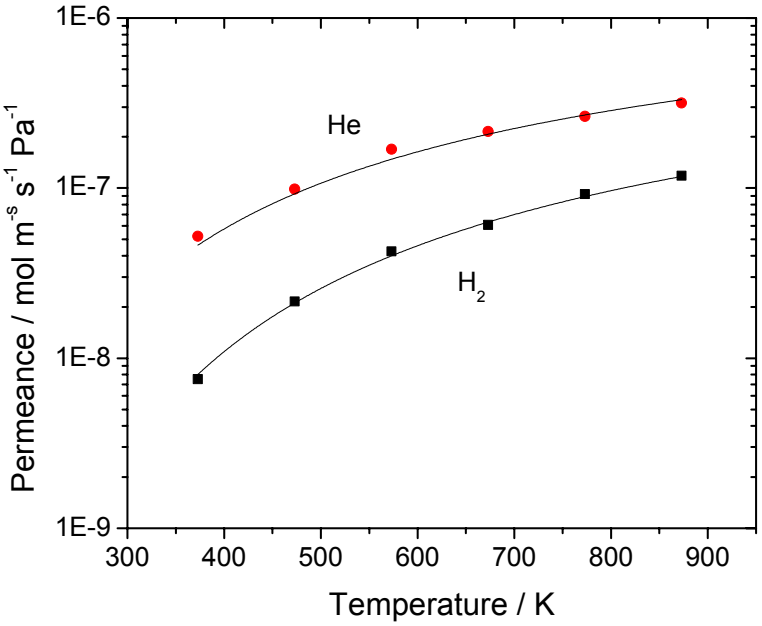

Figure 4.10. Statistical model calculated He and H_2 permeance on the silica membrane.

Points = Experimental values, Curves = Calculated values

Table 4.2. Best fit model parameters for the statistical gas permeance model (based on 20 nm of the silica layer thickness)

Gas	Number of solubility sites N_s (m^{-3})	Vibrational frequency ν^* (s^{-1})	Activation Energy ΔE_K (kJ mol^{-1})	Sum of least squares $\Sigma(Q_{calc.} - Q_{expl.})^2$
H_2	1.95×10^{27}	1.23×10^{13}	11.3	2.07×10^{-17}
He	3.81×10^{27}	7.77×10^{12}	8.0	8.09×10^{-16}

The best fit parameter values in the statistical jump equation are summarized in Table 4.2. The calculated vibrational frequency values at the doorway sites (ν^*) were 1.23×10^{13} s^{-1} for hydrogen and 7.77×10^{12} s^{-1} for helium, which are close to the vibrational frequency values at the solubility sites for silica glass reported in the literature ($H_2 = 1.22 \times 10^{13}$ s^{-1}, He = 6.90×10^{12} s^{-1}[8]). The calculated N_s values were 1.95×10^{27} sites m^{-3} for hydrogen and 3.81×10^{27} sites m^{-3} for helium, which are slightly higher than those reported for vitreous silica glass ($H_2 = 1.07 \times 10^{27}$ sites m^{-3} [15], He = 2.22×10^{27} sites m^{-3} [16]) . This makes sense since the structure of the silica layer formed by CVD in this work is expected to be more open than vitreous silica and to accommodate more sites. Note that the value of N_s is larger for He than for H_2. This is because on the average there are more sites that are able to accommodate the smaller He atom than the slightly larger H_2 molecule. The calculated activation energies (H_2 = 11.3 kJ mol^{-1}, He = 8.0 kJ mol^{-1}) were also in good agreement with the measured values (H_2 = 14.8 kJ mol^{-1}, He = 9.8 kJ mol^{-1}). The activation energies for small gas permeation through the silica layer obtained in this work are much lower than those for the vitreous silica glass reported in the literature (H_2 = 37.2 – 38.3 kJ mol^{-1} [11,12], He = 17.8 – 21.1 kJ mol^{-1} [13,14]), indicating that the doorway passageways in the silica layer are larger. The larger permeability of He over H_2 can thus be understood from the larger number of solubility sites for He, coupled with a lower jump barrier.

In summary, the results of this study indicated that the interstitial structure of silica obtained by CVD in this membrane is more open than in vitreous glass, and thus offers easier

diffusion of small gas molecules, resulting in high permeances for H_2 and He. The statistical jump analysis gave good simulated permeance results with physically realistic values for the number of solubility sites, vibrational frequency, and activation energy, which matched very well with experimental data.

4.4. Conclusions

A silica membrane was prepared on a porous alumina support by thermal decomposition of a silica precursor at 873 K in an inert atmosphere. After 12 h of silica deposition, the resulting composite membrane showed a high hydrogen permeance of the order of 10^{-7} mol m^{-2} s^{-1} Pa^{-1} at 873 K with H_2 selectivities over CH_4, CO, and CO_2 in excess of 2000. The gas permeance through the alumina support decreased with the inverse square root of temperature in accordance with a Knudsen permeation mechanism. The small gas permeance (He, and H_2) through the silica/alumina membrane was activated, and increased with temperature, and could be explained quantitatively by a statistical jump mechanism. The thickness of the silica layer obtained from FESEM experiments was about 20 – 30 nm. The surface structure of the membranes obtained by AFM measurements indicated that the surface became smooth after the silica layer deposition indicating a uniform silica film formation on the γ-Al_2O_3 surface of the alumina support. These results indicate that the high temperature chemical vapor deposition of silica by the thermal decomposition of TEOS applied in this work is excellent in controlling the thickness and uniformity of the silica layer formed on porous supports. The mechanism of small gas permeation through the silica membrane was described by a statistical gas permeance model originally presented for silica glass. The model analysis results gave good agreement with experimental gas permeance data using physically realistic values for the number of solubility sites (N_s), vibrational frequency of the molecules at the doorway sites (ν^*), and activation energy of permeation. The higher values in the number of solubility sites and low activation energies for the silica layer in this work compared to those for vitreous silica glasses indicated that the interstitial structure of the silica obtained from CVD is more open, thus accommodating more sorption sites for the small gas molecules and providing higher diffusivity. These give rise to high permeance for H_2 and He with hydrogen selectivities for CH_4, CO, and CO_2 over 2000 at 873 K.

References

[1] R.J.R. Uhlhorn, M.H.B.J. Huis In't Veld, K. Keizer, A. J. Burggraaf, *J. Mater. Sci.* **1992**, 27, 527.

[2] M. Knudsen, *Ann. Phys.* 1909, 28, 75.

[3] D. Lee, S. T. Oyama, *J. Membr. Sci.* **2002**, 210, 291.

[4] D.W. Breck, Zeolite Molecular Sieves: Structure, Chemistry and Use, Wiley, New York, **1974**, p.636.

[5] R.M. Barrer, D.E.W. Vaughan, *Trans. Faraday Soc.* **1967**, 63, 2275.

[6] J.S. Masaryk, R.M. Fulrath, *J. Chem. Phys.* **1973**, 59 (3), 1198.

[7] P.L. Studt, J.F. Shackelford, R.M. Fulrath, *J. Appl. Phys.* **1970**, 41, 2777.

[8] J.F. Shackelford, P.L. Studt, R.M. Fulrath, *J. Appl. Phys.* **1972**, 43, 1619.

[9] J.E. Dennis Jr., R.B. Schnabel, Numerical methods for unconstrained optimization and nonlinear equations, Prentice-Hall Inc., New Jersey, **1983**.

[10] J.F. Shackelford, J.S. Masaryk, *J. Non-Cryst. Solids*, **1978**, 30, 127.

[11] R.W. Lee, R.C. Frank, D.W. Swets, *J. Chem. Phys.* **1962**, 36, 1062.

[12] R.W. Lee, *J. Chem. Phys.* **1963**, 38, 448.

[13] J.E. Shelby, *J. Am. Ceram. Soc.* **1972**, 55, 61.

[14] J.E. Shelby, *J. Am. Ceram. Soc.* **1972**, 54, 125.

[15] J.E. Shelby, *J. Appl. Phys.* **1977**, 48, 3387.

[16] J.E. Shelby, *J. Appl. Phys.* **1976**, 47, 135.